HHS Public Access

Author manuscript

Cancer Res. Author manuscript; available in PMC 2021 August 15.

Published in final edited form as:

Cancer Res. 2021 February 15; 81(4): 1014–1025. doi:10.1158/0008-5472.CAN-20-1876.

Therapeutic Targeting of Metadherin Suppresses Colorectal and Lung Cancer Progression and Metastasis

Minhong Shen[1], **Shanshan Xie**[1,2,3,4], **Michelle Rowicki**[1], **Sven Michel**[5], **Yong Wei**[1], **Xiang Hang**[1], **Liling Wan**[1], **Xin Lu**[1], **Min Yuan**[1], **John F. Jin**[6], **Frank Jaschinski**[5], **Tianhua Zhou**[4,7,8], **Richard Klar**[5], **Yibin Kang**[1,9,10,*]

[1]Department of Molecular Biology, Princeton University, Princeton, NJ 08544, USA

[2]Department of Cell Biology, Zhejiang University School of Medicine, Hangzhou 310058, China

[3]The Children's Hospital, Zhejiang University School of Medicine, Hangzhou 310058, China

[4]Cancer Center, Zhejiang University, Zhejiang, China

[5]Secarna Pharmaceuticals GmbH & Co. KG, Am Klopferspitz 19, 82152 Planegg/Martinsried Germany

[6]Firebrand Therapeutics, 174 Nassau Street, #331, Princeton, NJ, 08542, USA

[7]Department of Cell Biology and Cancer Institute of the Second Affiliated Hospital, Zhejiang University School of Medicine, Hangzhou 310058, China

[8]Department of Molecular Genetics, University of Toronto, Toronto, ON M5S 1A8, Canada

[9]Cancer Metabolism and Growth Program, Rutgers Cancer Institute of New Jersey, New Brunswick, NJ, 08903, USA

[10]Lead Contact

Abstract

Colorectal and lung cancers account for one-third of all cancer-related deaths worldwide. Previous studies suggested that Metadherin (MTDH) is involved in the development of colorectal and lung cancers. However, how MTDH regulates the pathogenesis of these cancers remains largely unknown. Using genetically modified mouse models of spontaneous colorectal and lung cancers, we found that MTDH promotes cancer progression by facilitating Wnt activation and by inducing cytotoxic T cell exhaustion, respectively. Moreover, we developed locked nucleic acid-modified (LNA) MTDH antisense oligonucleotides (ASOs) that effectively and specifically suppress MTDH expression *in vitro* and *in vivo*. Treatments with MTDH ASOs in mouse models significantly attenuated progression and metastasis of colorectal, lung, and breast cancers. Our study opens a

[*]**Correspondence**: Yibin Kang, Ph.D., Department of Molecular Biology, Washington Road, LTL 255, Princeton University, Princeton, NJ 08544, Phone: (609) 258-8834; Fax: (609) 258-2340, ykang@princeton.edu.

Disclosure of Potential Conflicts of Interest

R. Klar, F. Jaschinski, S. Michel are employees of Secarna Pharmaceuticals GmbH & Co. KG. J. Jin is a co-founder and Y. Kang is a co-founder and chair of scientific advisory board of Firebrand Therapeutics Inc., which has licensed relevant technologies from Princeton University to develop MTDH-SND1 targeting therapeutics. Secarna and Firebrand have a collaborative agreement in the development of MTDH-targeting ASOs.

new avenue for developing therapies against colorectal and lung cancers by targeting MTDH using LNA-modified ASO.

Introduction

Lung cancer is the most common cancer type worldwide. Although the incidence of lung cancer continues to decline since the last decade, it still accounts for one-quarter of all cancer deaths (1). More than 80% of lung cancers are non-small cell lung cancer (NSCLC), of which adenocarcinoma, squamous cell carcinoma, and large cell carcinoma are the most common subtypes (2). Aided by increasingly sophisticated therapeutic strategies, such as targeted therapies (3) and immunotherapies (4), the clinical outcomes in NSCLC patients have significantly improved over the past two decades. However, given the molecular heterogeneity of the disease, the response rates of the current therapeutic strategies are usually low (5). Furthermore, treatment resistance is frequently observed (6), which reduces the clinical benefits of these treatments to patients. To overcome these challenges and increase the population that could potentially benefit from targeted therapies, identification of new driver genes that promote lung cancer progression and subsequent development of novel therapeutic strategies are urgently needed (7).

Following lung cancer, colorectal cancer is the second most common cause of cancer death in United States (8). More than 900,000 patients are predicted to die from this disease annually worldwide (9). Even worse, the incidence and mortality were gradually increasing in young patients (age<50) during the last decade (8). Similar to lung and other types of cancer, colorectal cancer is also a heterogeneous disease with multiple genetic and epigenetic aberrations (10). The earliest event that occurs in the development of colorectal cancer is the mutation of *Adenomatous polyposis coli* (*APC)* gene, which results in hyperactivation of Wnt signaling (11). About 90% of patients show *APC* mutations or allelic losses (12). Although Wnt signaling is essential for colorectal cancer progression, therapies that directly target key components in this pathway are not currently feasible given the broad side effects. Therapies that target angiogenesis or epidermal growth factor receptor (EGFR) provide marginal durable benefits in combination with chemotherapies. However, the overall response rate of these therapies is limited (13). It is therefore imperative to further explore the mechanisms underlying colorectal cancer progression and metastasis with the goal of developing new and effective therapeutic agents.

Metadherin (MTDH, also called AEG-1) has been found to be involved in the development of many types of cancer, including breast, prostate, liver, lung and colorectal cancers (14). Extensive studies of MTDH in liver (15,16), breast (17–19) and prostate (20) cancers established its key role in promoting tumor initiation, progression, metastasis and treatment resistance. Moreover, no apparent physiological defects were observed upon *Mtdh* knockout in mouse models, making it an attractive therapeutic target for cancer treatment (19). Previous *in vitro* studies on MTDH in lung and colorectal cancers resulted in contradictory conclusions (21–23). In this study, we thoroughly investigated the role of MTDH in lung and colorectal cancers using robust genetically modified mouse tumor models as well as xenograft/allograft models. In addition to revealing distinct functions of MTDH in

promoting colorectal and lung cancers, we developed LNA-modified MTDH-specific antisense oligonucleotides (ASOs), and extensively assessed their anti-cancer therapeutic potentials in pre-clinical models.

Materials and Methods

Animal Models

All procedures involving mice and experimental protocols were approved by the Institutional Animal Care and Use Committees (IACUC) of Princeton University. Mouse strains used in this study are listed in Supplementary Materials and Methods. For allograft and xenograft studies, 8-weeks immunocompromised NSG or immunocompetent C57BL/6 mice were used. For ASO treatment, ASOs were reconstituted with PBS and injected into mice intraperitoneally (i.p.) at a dose of 20 mg/kg. The treatment schemes are indicated in figures. Additional details and references are provided in the Supplementary Materials and Methods.

TCGA dataset analyses

Clinical data of colorectal adenocarcinoma and lung adenocarcinoma was downloaded from TCGA (Firehose Legacy) dataset in cBioportal (RRID:SCR_014555) website. The MTDH expression was determined by Agilent microarray and RNA-seq V2 RSEM in colorectal adenocarcinoma and lung adenocarcinoma, respectively. Patients without disease-free survival (DFS) information or MTDH expression data were excluded. DFS of colorectal adenocarcinoma and lung adenocarcinoma patients was then stratified by *MTDH* expression. The cutoffs were chosen automatically by R software with optimal p values.

Cell lines

HEK293T (RRID:CVCL_0063), SW620 (RRID:CVCL_0547), mouse breast cancer cell line 4T1 (RRID:CVCL_0125), mouse renal cell carcinoma cell line Renca (RRID:CVCL_2174), Lewis lung carcinoma cell line LLC1 (RRID:CVCL_4358) and L cells were grown in DMEM supplemented with 10% FBS and Pen/Strep. DLD1 (RRID:CVCL_0248) cells were grown in RPMI1640 supplemented with 10% FBS and Pen/Strep. MC-38 (RRID:CVCL_B288) cells were cultured with DMEM media supplemented with 10% FBS, 2mM glutamine, 0.1 mM nonessential amino acids, 1 mM sodium pyruvate, 10 mM Hepes, 50μg/ml gentamycin sulfate, and Pen/Strep. HEK293T, SW620, DLD1, 4T1, Renca, and LLC1 cells were purchased from ATCC. MC-38 cells were purchased from Kerafast. L cells were gift from the Devenport lab at Princeton University. All cell lines were authenticated through STR profiling and tested monthly for *Mycoplasma* by PCR. Cell lines were not passaged more than 30 times.

Immunoprecipitation (IP) and western blotting (WB) analysis

For the IP experiment, plasmids were transfected into HEK293T cells. The cells were then lysed and IP with indicated antibodies. Samples were subjected to western blotting (WB). For WB analysis, protein lysates were resolved with SDS-PAGE gel and immunoblotted with standard protocols. Details and references are provided in the Supplementary Materials and Methods.

3D culture

3D culture was performed as previously described (24). Details and references are provided in the Supplementary Materials and Methods.

Immunohistochemistry (IHC) staining.

Paraffin-embedded intestine and lung tumor samples were cut at a thickness of 4 μm. The slides were baked overnight at 60°C. Next, the tissue slides were washed with PBS after deparaffinization and hydration and then boiled in citrate buffer at 100°C for 40 min. After treatment with 3% H_2O_2 for 30 min to block endogenous peroxidase, slides were incubated at 4°C overnight with indicated antibodies. Antibodies and staining details are listed in Supplementary Materials and Methods.

Immunofluorescence (IF) staining

For paraffin-embedded liver samples, slides were prepared similarly as for IHC staining described above. For 3D cultured spheres, the samples were collected from dishes and Matrigel (Corning Matrigel Matrix) was digested as previously reported (25). Antibodies and staining details are listed in Supplementary Materials and Methods.

Adenovirus Cre intranasal infection

The infection was performed as previously described (26,27). Details and references are provided in the Supplementary Materials and Methods.

Flow cytometry

Dissociated lungs were dissected, and single cell suspensions were prepared as previously described (28). Antibodies and staining details are listed in Supplementary Materials and Methods. Gating strategy is shown in Supplementary Fig. S3D.

Intestine methylene blue staining

Intestines were collected from experimental mice, opened longitudinally and washed with PBS. The intestines were then fixed overnight with 10% formalin at room temperature. Meanwhile, 0.5% Methylene Blue Stain was prepared by dissolving 15 mg Methylene Blue (Sigma-Aldrich #M9140) in 30 mL of distilled water. Intestines were stained in 0.5% Methylene Blue Stain for 30 sec. The samples were rinsed with distilled water and examined with a dissecting microscope.

Antisense oligonucleotides

15-, 16- and 17-mer ASOs were selected based on the sequence of the mouse MTDH gene. LNA-modified nucleotides were inserted into the flanks of ASOs. Main criterion for sequence selection was selectivity to avoid undesired off-target effects. LNA-modified ASOs were ordered from Microsynth or Axolabs. For *in vitro* testing, ASOs were resuspended in H_2O, for *in vivo* experiments ASOs were resuspended in PBS. ASOs were added to cells *in vitro* without the use of a transfection reagent and used for *in vivo* studies without a delivery system. Sequences of selected MTDH ASOs and control oligonucleotide used in this study

are listed in Supplementary Table S1. Control oligonucleotide was derived from a previous study (29).

Investigation of *in vitro* efficacy of mouse MTDH-specific LNA-modified ASOs

Target knockdown efficacy of mouse MTDH-specific LNA-modified ASOs was investigated in 4T1 and Renca cells *in vitro* Details and references are provided in the Supplementary Materials and Methods.

TLR-9 activation assay

HEK293T cells stably transfected with a mouse TLR9/NFκB/Luciferase reporter plasmid were treated with different concentrations of the respective ASO or a positive control (ODN1668, Invivogen) for 24 hours. For detection of luciferase activity, ONE-Glo™ EX reagent (Promega) was added to the cells and luminescence was measured on a BMG Clariostar reader.

qRT-PCR analyses

Real-time RT-PCR was performed on an ABI 7900 96 HT series PCR machine (Applied Biosystems) using SYBR Green Supermix (Bio-Rad Laboratories). Primer sequences are listed in Supplementary Table S2.

Viral production, infection, and Wnt reporter assay

Virus were produced using HEK293T cells that detailed in Supplementary Materials and Methods

For Wnt reporter assay, the cells were treated with PBS, 500 ng/ml Wnt3a recombinant protein (R&D, #5036-WN), Wnt3a or control conditioned media that isolated from L cells as previously described (30). 6 hr after the treatment, Wnt activity was determined by firefly luciferase signal.

Statistical analyses

Results are reported as mean ± standard error of the mean (SEM). For *in vivo* liver, lung metastasis and primary tumor growth experiments, the number of mice in each group was indicated in each specific experiment. Survival curves were constructed using the Kaplan-Meier method and compared between subgroups with the log-rank test. All statistical analyses were done using GraphPad Prism 7 (RRID:SCR_002798). In instances where multiple comparisons were performed, Dunnett or Bonferroni correction was used, unless otherwise specified. Longitudinal models for analyzing the repeated measurements of tumor volume and body weight to test: a) whether there is a significant difference in the overall trend with a polynomial model and best fitted correlation structure among the repeated measurements; and b) whether the difference is significant at the last time-point. Specific tests are described in the respective figure legends. p values < 0.05 were considered statistically significant, with * $p < 0.05$, ** $p < 0.01$, *** $p < 0.001$, **** $p < 0.0001$, n.s.: not significant ($p > 0.05$), unless otherwise indicated in the figure.

Results

MTDH promotes colorectal cancer initiation, progression and metastasis

To study the function of MTDH in colorectal cancer using genetically modified mouse models, we obtained the *B6.Apc*$^{min/+}$ strain from Jackson Laboratory, which has been widely used to mimic *APC* mutation-induced gastrointestinal (GI) tract cancers (31,32). The strain was crossed to the *B6.Mtdh*$^{-/-}$ strain that we previously generated (19,20) to obtain *B6.Apc*$^{min/+}$ mice with and without endogenous *Mtdh* knockout (KO) (Fig. 1A). *Mtdh* KO significantly extended the lifespan of mice as compared to the *Mtdh* wild type strain (Fig. 1B). Consistently, *Mtdh* KO significantly reduced cancer development which is evidenced by less tumor nodules across the intestines (Fig. 1C and D), suggesting that MTDH is critical for GI tract cancer development.

To further validate these findings, we generated a human colorectal cancer cell line SW620 with endogenous MTDH knockdown (KD) by transducing the cells with lentiviruses expressing a short hairpin RNA (shRNA) targeting MTDH (Fig. 1E). The control and MTDH-KD SW620 cells were then injected subcutaneously into NSG mice to investigate primary tumor growth as well as spontaneous metastasis. MTDH-KD significantly delayed primary tumor progression *in vivo* (Fig. 1F–1H). Moreover, spontaneous liver metastasis was also notably attenuated upon MTDH KD (Fig. 1I). Next, we performed intrasplenic injections to directly investigate the role of MTDH in experimental liver metastasis. NSG mice that were injected with control SW620 cells generated significantly more liver metastatic nodules than MTDH-KD cells (Fig. 1J and K). The results were confirmed with another colorectal cancer cell line DLD1 (Supplementary Fig. S1A–S1F). These findings were consistent with prognosis analysis of *MTDH* in the TCGA colorectal cancer dataset. Patients with high level of *MTDH* expressed in their tumors experienced significantly worse disease-free survival (Supplementary Fig. S1G). Overall, these data indicated that MTDH enhances colorectal cancer growth and metastasis.

MTDH elevates Wnt activation by facilitating nuclear localization of β-catenin

Next, we investigated how MTDH enhances intestinal/colorectal cancer development. Intestinal samples collected from *B6.Apc*$^{min/+}$*;Mtdh*$^{+/+}$ (WT), *B6.Apc*$^{min/+}$*;Mtdh*$^{+/-}$ (HET), or *B6.Apc*$^{min/+}$*;Mtdh*$^{-/-}$ (KO) mice were subjected to immunohistochemistry (IHC) staining of Ki67. The results indicated that MTDH promotes tumor proliferation (Fig. 2A and B), as indicated by number of Ki67-positive cells. However, no difference in terms of cancer cell survival was observed which is indicated by cleaved caspase-3 (CC-3) staining (Supplementary Fig. S2A and S2B).

To further explore the underlying mechanism, we established an *in vitro* 3D culture assay using human SW620 colorectal cancer cells. Consistent with the high proliferation rate that we observed in *B6.Apc*$^{min/+}$*;Mtdh*$^{+/+}$ mice, control SW620 cells formed more and bigger tumorspheres in our 3D culture system than MTDH-KD cells (Fig. 2C and D). Previous studies have established Wnt signaling as the most frequently altered and hyperactivated pathway in colorectal cancer (33,34). We next investigated if MTDH is involved in Wnt signaling activation. To this end, we stably expressed the 7xTcf-FFluc Wnt reporter (35) in

control and MTDH-KD SW620 cells. We observed a lower basal Wnt signaling activity in MTDH-KD cells than control cells, and moreover, less activation of the reporter in response to Wnt3a stimulation (Fig. 2E). These results suggested that MTDH may be required for optimal Wnt activation in colon cancer.

SW620 tumors from experiment in Fig. 1F were further analyzed to validate these *in vitro* findings. Many Wnt signaling downstream targets were found to be down-regulated in MTDH-KD tumors (Fig. 2F; Supplementary Fig. S2C), suggesting reduced Wnt signaling activity *in vivo* upon MTDH loss. Previous studies indicated that MTDH could be involved in β-catenin nuclear translocation in other cancer types (36,37), which is the key step of Wnt activation. Consistent with this notion, we observed significantly less nuclear β-catenin in MTDH-KD colorectal cancer 3D culture spheres (Fig. 2G; Supplementary Fig. S2D and S2E). The finding was also validated by our *in vivo* liver metastatic samples and spontaneous mouse model, which again showed weaker nuclear localization of β-catenin upon MTDH knockdown and knockout (Supplementary Fig. S2F–S2I). Moreover, immunoprecipitation assay indicated that MTDH interacts directly with β-catenin (Fig. 2H). Of note, MTDH has stronger interaction with S33Y and S33A/S37A/S45A mutant forms of β-catenin, which mimic the activated forms of β-catenin (29) (Fig. 2H). Collectively, these results show that MTDH binds to β-catenin, especially its activated forms, and facilitates its nuclear translocation. As a result, Wnt signaling was enhanced to promote colorectal cancer growth, progression and metastasis.

MTDH accelerates lung cancer progression

Taking advantage of the same *Mtdh* KO mouse model, we also explored the function of MTDH in lung cancer development. To this end, we employed the *B6.KRAS-G12D*$^{fl/+}$ model, which is a widely used mouse model of K-Ras-induced lung adenocarcinoma (38). Endogenous *Mtdh* was knocked out in the strain by crossing it with our *B6.Mtdh*$^{-/-}$ mouse model (Fig. 3A). The *B6.KRAS-G12D*$^{fl/+}$;*Mtdh*$^{+/+}$ (WT), *B6.KRAS-G12D*$^{fl/+}$;*Mtdh*$^{+/-}$ (HET), and *B6.KRAS-G12D*$^{fl/+}$;*Mtdh*$^{-/-}$ (KO) mice were randomized and were subjected to intranasal infection with adenovirus Cre (27) to specifically induce KRAS-G12D expression in the lungs and initiates lung cancer development. Mice that maintained WT *Mtdh* expression had a significantly worse survival rate after adenovirus Cre infection (Fig. 3B) as compared to *Mtdh* HET and *Mtdh* KO mice. Consistently, wild type mice had heavier lung tumor burden compared with *Mtdh* KO and *Mtdh* HET mice (Fig. 3C–3E), suggesting that MTDH promotes lung cancer progression.

We also used the mouse Lewis lung carcinoma cell line LLC1, which was established from the lung of a C57BL/6 mouse (39) to confirm the results that we observed in the genetic KRAS mouse model. This cell line is highly tumorigenic and elicits significant anti-tumor immune response, and has been widely used as a syngeneic mouse model to evaluate therapeutic efficacy for lung cancer *in vivo* (40–44). We generated LLC1 cells with endogenous MTDH KD (Fig. 3F) and injected these cells into C57BL/6 mice to investigate lung cancer progression. As expected, mice injected with MTDH-KD cells developed fewer tumors in lungs and had improved survival rates than mice injected with control cells (Fig. 3G and H). Consistently, lung adenocarcinoma patients with low *MTDH* expression in their

tumors have significantly better disease-free survival based on the analysis of the TCGA dataset (Supplementary Fig. S3A).

MTDH elevates lung cancer progression by suppressing anti-tumor immune response

Next, we asked whether MTDH enhances lung cancer progression also through facilitating β-catenin nuclear translocation and enhancing Wnt signaling. To address this question, we performed Wnt reporter assay in LLC1 cells with or without MTDH KD. We did not observe different Wnt activation at basal level upon MTDH KD. However, MTDH KD significantly inhibited Wnt activation when the cells were treated with Wnt3a conditioned media (Supplementary Fig. S3B), suggesting that MTDH KD also attenuates Wnt activation in lung cancer cells *in vitro*. Moreover, we observed less tumor sphere formation after MTDH KD (Supplementary Fig. S3C). To further confirm these findings *in vivo*, lung tumors formed by control or MTDH KD LLC1 cells were collected for IHC staining to investigate the nuclear translocation of β-catenin. To our surprise, although there is a trend toward reduced nuclear β-catenin upon MTDH KD, this difference did not reach statistical significance (Supplementary Fig. S3D). Moreover, the overall ratio of nuclear localized β-catenin is low in the lung tumor sections (Supplementary Fig. S3D), indicating that Wnt/β-catenin signaling may not play a key role in LLC lung cancer progression *in vivo*. Consistent with this notion, it has been reported that Wnt hyperactivation is not the main cause of lung cancer in the clinic (45). Taken together, although MTDH may enhance Wnt activation upon induction *in vitro*, the lung cancer-promoting role of MTDH may be mediated by other mechanisms *in vivo*.

Given the facts that lung is an inflammatory organ with pronounced immune cell infiltration (46) and immune checkpoint blockade therapy has achieved great success in lung cancer (47), we asked if MTDH affects T cell infiltration into tumors. To this end, lungs with tumors from the *B6.KRAS-G12D*$^{fl/+}$ model were collected to analyze T cell populations. MTDH KO significantly increased T cell infiltration, especially CD8$^+$ cytotoxic T cells that are mainly responsible for tumor clearance (Fig. 4A, gating strategy in Supplementary Fig. S3E). The elevated T cell infiltration in lung tumors with MTDH KO was also confirmed with IHC staining (Supplementary Fig. S3F and S3G). Moreover, lungs with MTDH KO have significantly fewer PD-1 expressing CD8$^+$ T cells (Fig. 4A, right panel). On the other hand, we observed less PD-L1 expression in tumor samples upon MTDH KO (Fig. 4B), suggesting MTDH KO tumors may experience less T cell exhaustion. These findings were further validated by immunostaining of LLC1 tumors which again showed that MTDH KD enhanced T cell infiltration, reduced PD-1$^+$ cells, and down-regulated PD-L1 expression in tumors (Fig. 4C and D). Collectively, our results indicate that MTDH promotes lung cancer progression by inducing PD-1/PD-L1 expression, and as a result, decreasing cytotoxic T cell infiltration.

As observed above, MTDH-induced lung cancer is mediated by decreasing cytotoxic T cell infiltration. In addition to Wnt/β-Catenin pathway, we asked if such alteration of immune cell population as compared to MTDH KO also contributes to colorectal cancer progression. To this end, we collected intestine samples from age-matched *B6. Apc*$^{min/+}$*;Mtdh*$^{+/+}$ (WT) and *B6. Apc*$^{min/+}$*;Mtdh*$^{-/-}$ (KO) mice and performed IHC staining of CD3, CD8, PD-1 and

PD-L1. We did not detect any significant difference between MTDH WT and KO mice in terms of the numbers of $CD3^+$, $CD8^+$, and PD-$L1^+$ cells in tumors (Supplementary Fig. S3H and S3I). Interestingly, we did not observe any PD-1^+ cells in either MTDH WT or KO samples (Supplementary Fig. S3H). Moreover, in general, we observed much less overall $CD3^+$ and $CD8^+$ T cell infiltration compared with lung tumor models (Fig. 4C and D; Supplementary Fig. S3H and S3I), suggesting immune cell regulation may not be a major contributing factor to the tumor-promoting function of MTDH in colorectal cancer, at least in the mouse model used in our current study. Collectively, the results indicate that MTDH promotes lung and colorectal cancers progression and metastasis through two distinct mechanisms.

Identification of LNA-modified antisense oligonucleotides (ASOs) targeting MTDH

The tumor promoting role of MTDH in colorectal and lung cancers in the current study, as well as results from other cancer models (19,20) established it as a potentially novel target for cancer therapy (14). To evaluate the therapeutic potential of targeting MTDH, we developed a set of LNA-modified ASOs with potent MTDH-targeting activity *in vitro* and *in vivo.* LNA-modified ASOs against MTDH were designed *in silico* with a focus on target selectivity to avoid undesired off-target effects. A set of 104 LNA-modified ASOs were screened with regard to target knockdown efficacy in 4T1 and Renca cells at a final concentration of 5 μM without the use of a transfection reagent. *Mtdh* mRNA expression was potently inhibited in both cell lines by MTDH-specific LNA-modified ASOs (Supplementary Fig. S4A). There was a significant correlation in the activity of ASOs in both tested cell lines. Of note, treatment of cells with a control oligonucleotide did not result in any reduction of *Mtdh* mRNA expression (Supplementary Fig. S4A). We selected five top ASOs that inhibited *Mtdh* mRNA expression by > 90% (represented by a residual *Mtdh* mRNA expression of < 0.1) and investigated the dose-dependency of target knockdown in 4T1 cells. All candidates reduced *Mtdh* mRNA expression in a dose-dependent manner with IC_{50} values in the low nanomolar range (Supplementary Fig. S4B). The KD efficacy of the ASOs was also validated at the protein level in colorectal and lung cancer cell lines, in addition to the 4T1 cell line (Fig. 5A; Supplementary Fig. S4C).

It has been shown in the past that ASOs can have pro-inflammatory potential, e.g. by activating TLR9 (48). We therefore investigated the pro-inflammatory potential of the five ASOs using a reporter assay and did not observe TLR9 activation (Fig. 5B), which supports the feasibility for *in vivo* treatment. Three ASOs, A34051Mi, A34068Mi, and A34082Mi were next selected for extensive assessment of *in vivo* tolerability. To this end, we designed a treatment scheme based on our experiences that we gathered in the past for the tolerability study (Supplementary Fig. S4D). Specifically, there is a loading phase with 5 consecutive injections in the first week (days 0–6) followed by maintenance in the second week (days 7–13), with a one-day break in between each of 3 injections. The loading phase is beneficial for the efficacy of ASOs as this leads to saturation of the liver and the kidney where most of the ASOs end up. The mice were then treated with these ASOs using the treatment regimen. Body weight was measured daily starting on the day of treatment initiation and liver damage was evaluated at endpoint to monitor potential toxicity. Among these ASOs, only A34068Mi induced significant body weight loss across the treatment (Fig. 5C). Consistently, high liver

toxicity was observed in the mice treated with A34068Mi as measured by serum ALT and AST levels (Fig. 5D). Taken together, we selected A34051Mi and A34082Mi for further studies as they could effectively knockdown MTDH with minimal toxicity *in vivo*.

Treatment of mice with unformulated MTDH-specific LNA-modified ASOs inhibits progression and metastasis of multiple cancers

To evaluate the therapeutic potential of the two selected MTDH LNA-modified ASOs, an optimal *in vivo* treatment scheme was designed based on a previously reported study (49). A34051Mi was selected to validate the MTDH KD efficiency *in vivo* with the treatment scheme (Supplementary Fig. S5A). Considering the extensive functional studies of MTDH that have been done on breast cancer (17–20,50), we chose a breast cancer model to start with the *in vivo* treatment to determine the *in vivo* MTDH KD efficiency. Mice bearing 4T1 primary mammary gland tumors were treated as indicated in Supplementary Fig. S5A. At the end of the treatment, primary tumors were collected and MTDH KD efficiency was evaluated with qRT-PCR and western blot. As we expected, MTDH mRNA and protein levels were effectively reduced *in vivo* upon the treatment (Supplementary Fig. S5B and S5C). We therefore adapted the treatment scheme that includes 5 consecutive injections as a loading phase in the first week followed by a maintenance phase of 3 consecutive injections in each week for the subsequent experimental therapeutic studies (Supplementary Fig. S5D).

Next, we started the therapeutic evaluation in a breast cancer model. Mice bearing 4T1 primary tumors with size of ~2 mm in diameter were randomized into three groups and treated with the negative control oligonucleotide or the two MTDH-specific ASOs, A34051Mi and A34082Mi. A34051Mi and A34082Mi treatments significantly inhibited primary tumor growth as well as spontaneous lung and liver metastasis (Supplementary Fig. S6A–S6C). MTDH KD was confirmed with western blot in tumors from mice that had been treated with A34051Mi and A34082Mi (Supplementary Fig. S6D). Next, we extended our treatments to colorectal and lung cancer models. Mice bearing MC-38 and LLC1 tumors, which represent colorectal and lung cancer respectively, were treated with control ASO, A34051Mi, or A34082Mi. A34051Mi and A34082Mi treatments significantly suppressed tumor progression (Fig. 6A, B, E, and F) as well as liver and lung metastasis (Fig. 6C; Supplementary Fig. S6E), and significantly extended the survival in the LLC1 model (Fig. 6G). To directly assess the anti-metastasis effect of ASOs, we performed tail vein injection of 4T1 cells and intrasplenic injection of MC-38 cells to develop experimental lung and liver metastasis respectively. After metastases were established, mice were treated with control ASO or A34051Mi and A34082Mi with the same scheme as shown in Supplementary Fig. S5D. The development of metastasis was monitored weekly by *in vivo* BLI. Significant reduction of lung and liver metastasis was observed upon MTDH-ASOs treatments (Supplementary Fig. S6F–S6I), confirming their anti-metastasis therapeutic effects. Consistently, western blot and IHC staining of MC-38 and LLC1 tumor samples validated potent knockdown of MTDH in tumors upon A34051Mi and A34082Mi treatments (Fig. 6D and H). Collectively, our data established the therapeutic potential of targeting MTDH with LNA-modified ASOs.

To further validate that the tumor-suppressive effect upon A34051Mi and A34082Mi treatments were caused specifically by MTDH targeting, MC-38 cells treated with the control oligonucleotide or the MTDH-specific ASOs A34051Mi or A34082Mi were subjected to the Wnt reporter assay *in vitro*. Consistent with what we observed in stable MTDH KD cells (Fig. 2E), A34051Mi and A34082Mi treatment also attenuated Wnt activation (Fig. 7A). Consistently, MC-38 tumors from animals treated with A34051Mi and A34082Mi showed significantly lower expression of Wnt downstream genes (Fig. 7B). These results indicate that A34051Mi and A34082Mi suppress Wnt activation in colorectal cancer by targeting MTDH. Similar to what we observed in Mtdh knockout mice, A34051Mi and A34082Mi decreased PD-L1 expression in lung tumors, reduced PD-1^+ cells, and increased cytotoxic T cell infiltration in LLC1 tumors (Fig. 7C and D). Taken together, these results confirm that MTDH-specific LNA-modified ASOs (A34051Mi and A34082Mi) suppress colorectal and lung cancer progression and metastasis by specifically reducing the expression of MTDH.

Discussion

In this study, we extensively explored the functions of MTDH in lung and colorectal cancers with both genetically modified spontaneous tumor models and xenograft/allograft models. The results indicate that MTDH promotes lung and colorectal cancer progression and metastasis with distinct mechanisms. More importantly, we identified MTDH-specific LNA-modified ASOs that potently inhibit MTDH expression *in vivo.* Targeting MTDH with LNA-modified ASOs significantly inhibits lung and colorectal cancer progression and metastasis, suggesting MTDH-specific ASOs as a promising therapeutic strategy to treat lung, colorectal, breast and other cancers.

Previous studies indicated that MTDH is upregulated during colorectal cancer progression in patients (51). Its genetic variants have also been observed in colorectal cancer patient samples (52), indicating that MTDH is involved in colorectal cancer progression. *In vitro* studies also revealed that MTDH promotes the tumorigenesis and migration of colorectal carcinoma cells (53,54). Consistent with these *in vitro* findings and clinical correlations, our genetic model of spontaneous mouse intestinal cancer models that mimic Wnt-induced colorectal cancer in patients showed a critical role of MTDH for cancer progression and metastasis *in vivo* (Fig. 1). Mechanistically, MTDH binds to and facilitates β-catenin nuclear translocation, and thus, elevates the activation of Wnt signaling. Consistent with our findings, positive correlation between MTDH and nuclear location of β-catenin has also been observed in patient samples (54). Moreover, MTDH high expression is correlated with worse survival in colorectal cancer patients (Supplementary Fig. S1G).

The involvement of MTDH in Wnt/β-catenin signaling has not only been identified in colorectal cancer, but also in other cancers, such as glioma (37), liver cancer (36,55), and gastric cancer (56). However, in liver and gastric cancers, MTDH activates Wnt signaling by upregulating the expression of LEF1 or β-catenin (55,56) rather than by directly binding to and facilitating the nuclear translocation of β-catenin. In our study, we observed a direct interaction of MTDH with β-catenin, which is consistent with previous studies (37,54). Moreover, we found that MTDH binds even stronger to activate β-catenin (Fig. 2H). Taken

together, the findings from our study and others established a key role of MTDH for Wnt activation by facilitating the nuclear translocation of activated β-catenin during colorectal cancer progression and metastasis.

In addition to Wnt/β-catenin signaling, other pathways, such as NF-κB (51), apoptosis (19,22), and AMPK (53) have also been proposed to explain the MTDH-dependent promotion of cancer development. These findings suggest a multifaceted role of MTDH in affecting multiple cancer-related pathways and functions during tumor progression in diverse cancer types. In line with this notion, we found that MTDH promotes lung cancer progression by suppressing T cell infiltration, which is distinct from its role in colorectal cancer. Moreover, given the fact that we observed reduced PD-L1 expressions in MTDH-KD LLC1 tumors, in which the host MTDH has not been altered, we believe that MTDH-induced reduction of cytotoxic T infiltration is likely through a tumor intrinsic pathway. However, we cannot exclude the possibility that stroma MTDH may also be involved in regulating T cell response to tumors, which may be a subject of investigation in future studies.

After having established the role of MTDH in colorectal and lung cancer progression and metastasis, we sought to therapeutically target MTDH using LNA-modified ASOs. To this end, we designed a set of ASOs as Gapmers that contain a central “gap” of DNA monomers flanked by LNA-modified nucleotides. The central “gap” recruits the cellular enzyme RNase H, which cleaves the target RNA upon binding. The ASOs that we used have a fully phosphorothioate (PTO) backbone, which makes them resistant to enzymatic degradation (57). As described in a previous study (49), we also observed potent activity of MTDH-specific ASOs *in vitro* without the use of a transfection reagent and *in vivo* without a delivery system. Both lung and colorectal cancer progression and metastasis were significantly suppressed upon treatment with MTDH-specific ASOs in mouse models. In parallel, given the tumor-promoting role of MTDH in breast cancer that we identified in our previous studies (17–19), we also tested the susceptibility of a breast cancer model for treatment with MTDH-specific ASOs. As expected, the selected MTDH ASOs significantly inhibited primary tumor growth and metastasis, suggesting the therapeutic potential of these ASOs could extend to other cancer types in which MTDH is required for tumor progression and metastasis. Moreover, the suppression of Wnt signaling and elevation of T cell infiltration upon MTDH ASO treatments confirms the on-target effects of these ASOs mechanistically. Taken together, our study thoroughly elucidated the function of MTDH in lung and colorectal cancers. Furthermore, we validated the therapeutic potential of LNA-modified ASOs targeting MTDH, which could be further developed to benefit patients with lung, colorectal, breast and other types of cancer in the future.

Supplementary Material

Refer to Web version on PubMed Central for supplementary material.

Acknowledgements

We thank N. Aiello, R. Gunaratna, M. Esposito and other lab members for technical supports and helpful discussions. We thank C. DeCoste and K. Rittenbach at the Molecular Biology Flow Cytometry Resource Facility

of Princeton University for flow cytometry assays. This research was supported by the Brewster Foundation and grants from the U. S. Department of Defense (BC123187) and American Cancer Society (RP-19-180-01-CSM) to Y. Kang, and postdoctoral fellowships from Susan G. Komen (PDF17332118) and NJCCR (DFHS15PPCO21) to M. Shen. This research was also supported by the Pre-clinical Imaging and Flow Cytometry Shared Resources of the Rutgers Cancer Institute of New Jersey (P30CA072720).

References

1. Siegel RL, Miller KD, Jemal A. Cancer statistics, 2020. CA Cancer J Clin 2020;70(1):7–30 doi 10.3322/caac.21590. [PubMed: 31912902]
2. Molina JR, Yang P, Cassivi SD, Schild SE, Adjei AA. Non-small cell lung cancer: epidemiology, risk factors, treatment, and survivorship. Mayo Clin Proc 2008;83(5):584–94 doi 10.4065/83.5.584. [PubMed: 18452692]
3. Chan BA, Hughes BG. Targeted therapy for non-small cell lung cancer: current standards and the promise of the future. Transl Lung Cancer Res 2015;4(1):36–54 doi 10.3978/j.issn.2218-6751.2014.05.01. [PubMed: 25806345]
4. Rolfo C, Caglevic C, Santarpia M, Araujo A, Giovannetti E, Gallardo CD, et al. Immunotherapy in NSCLC: A Promising and Revolutionary Weapon. Adv Exp Med Biol 2017;995:97–125 doi 10.1007/978-3-319-53156-4_5. [PubMed: 28321814]
5. Johnson KR, Ringland C, Stokes BJ, Anthony DM, Freemantle N, Irs A, et al. Response rate or time to progression as predictors of survival in trials of metastatic colorectal cancer or non-small-cell lung cancer: a meta-analysis. Lancet Oncol 2006;7(9):741–6 doi 10.1016/S1470-2045(06)70800-2. [PubMed: 16945769]
6. Morgillo F, Della Corte CM, Fasano M, Ciardiello F. Mechanisms of resistance to EGFR-targeted drugs: lung cancer. ESMO Open 2016;1(3):e000060 doi 10.1136/esmoopen-2016-000060. [PubMed: 27843613]
7. Herbst RS, Morgensztern D, Boshoff C. The biology and management of non-small cell lung cancer. Nature 2018;553(7689):446–54 doi 10.1038/nature25183. [PubMed: 29364287]
8. Siegel RL, Miller KD, Goding Sauer A, Fedewa SA, Butterly LF, Anderson JC, et al. Colorectal cancer statistics, 2020. CA Cancer J Clin 2020 doi 10.3322/caac.21601.
9. Collaborators GBDCC. The global, regional, and national burden of colorectal cancer and its attributable risk factors in 195 countries and territories, 1990–2017: a systematic analysis for the Global Burden of Disease Study 2017. Lancet Gastroenterol Hepatol 2019;4(12):913–33 doi 10.1016/S2468-1253(19)30345-0. [PubMed: 31648977]
10. Nguyen HT, Duong HQ. The molecular characteristics of colorectal cancer: Implications for diagnosis and therapy. Oncol Lett 2018;16(1):9–18 doi 10.3892/ol.2018.8679. [PubMed: 29928381]
11. Powell SM, Zilz N, Beazer-Barclay Y, Bryan TM, Hamilton SR, Thibodeau SN, et al. APC mutations occur early during colorectal tumorigenesis. Nature 1992;359(6392):235–7 doi 10.1038/359235a0. [PubMed: 1528264]
12. Coppede F, Lopomo A, Spisni R, Migliore L. Genetic and epigenetic biomarkers for diagnosis, prognosis and treatment of colorectal cancer. World J Gastroenterol 2014;20(4):943–56 doi 10.3748/wjg.v20.i4.943. [PubMed: 24574767]
13. Piawah S, Venook AP. Targeted therapy for colorectal cancer metastases: A review of current methods of molecularly targeted therapy and the use of tumor biomarkers in the treatment of metastatic colorectal cancer. Cancer 2019;125(23):4139–47 doi 10.1002/cncr.32163. [PubMed: 31433498]
14. Dhiman G, Srivastava N, Goyal M, Rakha E, Lothion-Roy J, Mongan NP, et al. Metadherin: A Therapeutic Target in Multiple Cancers. Front Oncol 2019;9:349 doi 10.3389/fonc.2019.00349. [PubMed: 31131259]
15. Sarkar D AEG-1/MTDH/LYRIC in liver cancer. Adv Cancer Res 2013;120:193–221 doi 10.1016/B978-0-12-401676-7.00007-3. [PubMed: 23889992]
16. Zhu K, Dai Z, Pan Q, Wang Z, Yang GH, Yu L, et al. Metadherin promotes hepatocellular carcinoma metastasis through induction of epithelial-mesenchymal transition. Clin Cancer Res 2011;17(23):7294–302 doi 10.1158/1078-0432.CCR-11-1327. [PubMed: 21976539]

17. Hu G, Chong RA, Yang Q, Wei Y, Blanco MA, Li F, et al. MTDH activation by 8q22 genomic gain promotes chemoresistance and metastasis of poor-prognosis breast cancer. Cancer Cell 2009;15(1):9–20 doi 10.1016/j.ccr.2008.11.013. [PubMed: 19111877]
18. Guo F, Wan L, Zheng A, Stanevich V, Wei Y, Satyshur KA, et al. Structural insights into the tumor-promoting function of the MTDH-SND1 complex. Cell Rep 2014;8(6):1704–13 doi 10.1016/j.celrep.2014.08.033. [PubMed: 25242325]
19. Wan L, Lu X, Yuan S, Wei Y, Guo F, Shen M, et al. MTDH-SND1 interaction is crucial for expansion and activity of tumor-initiating cells in diverse oncogene- and carcinogen-induced mammary tumors. Cancer Cell 2014;26(1):92–105 doi 10.1016/j.ccr.2014.04.027. [PubMed: 24981741]
20. Wan L, Hu G, Wei Y, Yuan M, Bronson RT, Yang Q, et al. Genetic ablation of metadherin inhibits autochthonous prostate cancer progression and metastasis. Cancer Res 2014;74(18):5336–47 doi 10.1158/0008-5472.CAN-14-1349. [PubMed: 25074613]
21. Yao Y, Gu X, Liu H, Wu G, Yuan D, Yang X, et al. Metadherin regulates proliferation and metastasis via actin cytoskeletal remodelling in non-small cell lung cancer. Br J Cancer 2014;111(2):355–64 doi 10.1038/bjc.2014.267. [PubMed: 24918821]
22. Li JW, Huang CZ, Li JH, Yuan JH, Chen QH, Zhang WF, et al. Knockdown of metadherin inhibits cell proliferation and migration in colorectal cancer. Oncol Rep 2018;40(4):2215–23 doi 10.3892/or.2018.6581. [PubMed: 30015962]
23. Ke ZF, Mao X, Zeng C, He S, Li S, Wang LT. AEG-1 expression characteristics in human non-small cell lung cancer and its relationship with apoptosis. Med Oncol 2013;30(1):383 doi 10.1007/s12032-012-0383-9. [PubMed: 23307243]
24. Lee GY, Kenny PA, Lee EH, Bissell MJ. Three-dimensional culture models of normal and malignant breast epithelial cells. Nat Methods 2007;4(4):359–65 doi 10.1038/nmeth1015. [PubMed: 17396127]
25. Vidi PA, Bissell MJ, Lelievre SA. Three-dimensional culture of human breast epithelial cells: the how and the why. Methods Mol Biol 2013;945:193–219 doi 10.1007/978-1-62703-125-7_13. [PubMed: 23097109]
26. Gierut JJ, Jacks TE, Haigis KM. In vivo delivery of lenti-Cre or adeno-Cre into mice using intranasal instillation. Cold Spring Harb Protoc 2014;2014(3):307–9 doi 10.1101/pdb.prot073445. [PubMed: 24591689]
27. DuPage M, Dooley AL, Jacks T. Conditional mouse lung cancer models using adenoviral or lentiviral delivery of Cre recombinase. Nat Protoc 2009;4(7):1064–72 doi 10.1038/nprot.2009.95. [PubMed: 19561589]
28. Chakrabarti R, Wei Y, Hwang J, Hang X, Andres Blanco M, Choudhury A, et al. DeltaNp63 promotes stem cell activity in mammary gland development and basal-like breast cancer by enhancing Fzd7 expression and Wnt signalling. Nat Cell Biol 2014;16(10):1004–15, 1–13 doi 10.1038/ncb3040. [PubMed: 25241036]
29. Jaschinski F, Korhonen H, Janicot M. Design and Selection of Antisense Oligonucleotides Targeting Transforming Growth Factor Beta (TGF-beta) Isoform mRNAs for the Treatment of Solid Tumors. Methods Mol Biol 2015;1317:137–51 doi 10.1007/978-1-4939-2727-2_9. [PubMed: 26072406]
30. Esposito M, Mondal N, Greco TM, Wei Y, Spadazzi C, Lin SC, et al. Bone vascular niche E-selectin induces mesenchymal-epithelial transition and Wnt activation in cancer cells to promote bone metastasis. Nat Cell Biol 2019;21(5):627–39 doi 10.1038/s41556-019-0309-2. [PubMed: 30988423]
31. Karim BO, Huso DL. Mouse models for colorectal cancer. Am J Cancer Res 2013;3(3):240–50. [PubMed: 23841024]
32. Taketo MM, Edelmann W. Mouse models of colon cancer. Gastroenterology 2009;136(3):780–98 doi 10.1053/j.gastro.2008.12.049. [PubMed: 19263594]
33. Schneikert J, Behrens J. The canonical Wnt signalling pathway and its APC partner in colon cancer development. Gut 2007;56(3):417–25 doi 10.1136/gut.2006.093310. [PubMed: 16840506]
34. Zhan T, Rindtorff N, Boutros M. Wnt signaling in cancer. Oncogene 2017;36(11):1461–73 doi 10.1038/onc.2016.304.. [PubMed: 27617575]

35. Fuerer C, Nusse R. Lentiviral vectors to probe and manipulate the Wnt signaling pathway. PLoS One 2010;5(2):e9370 doi 10.1371/journal.pone.0009370. [PubMed: 20186325]
36. Zhu K, Peng Y, Hu J, Zhan H, Yang L, Gao Q, et al. Metadherin-PRMT5 complex enhances the metastasis of hepatocellular carcinoma through the WNT-beta-catenin signaling pathway. Carcinogenesis 2019 doi 10.1093/carcin/bgz065.
37. Hu B, Emdad L, Kegelman TP, Shen XN, Das SK, Sarkar D, et al. Astrocyte Elevated Gene-1 Regulates beta-Catenin Signaling to Maintain Glioma Stem-like Stemness and Self-Renewal. Mol Cancer Res 2017;15(2):225–33 doi 10.1158/1541-7786.MCR-16-0239. [PubMed: 27903708]
38. Jackson EL, Willis N, Mercer K, Bronson RT, Crowley D, Montoya R, et al. Analysis of lung tumor initiation and progression using conditional expression of oncogenic K-ras. Genes Dev 2001;15(24):3243–8 doi 10.1101/gad.943001. [PubMed: 11751630]
39. Kellar A, Egan C, Morris D. Preclinical Murine Models for Lung Cancer: Clinical Trial Applications. Biomed Res Int 2015;2015:621324 doi 10.1155/2015/621324. [PubMed: 26064932]
40. Liu C, Zheng S, Jin R, Wang X, Wang F, Zang R, et al. The superior efficacy of anti-PD-1/PD-L1 immunotherapy in KRAS-mutant non-small cell lung cancer that correlates with an inflammatory phenotype and increased immunogenicity. Cancer Lett 2020;470:95–105 doi 10.1016/j.canlet.2019.10.027. [PubMed: 31644929]
41. Mittal R, Chen CW, Lyons JD, Margoles LM, Liang Z, Coopersmith CM, et al. Murine lung cancer induces generalized T-cell exhaustion. J Surg Res 2015;195(2):541–9 doi 10.1016/j.jss.2015.02.004. [PubMed: 25748104]
42. Pan J, Zhang Q, Sei S, Shoemaker RH, Lubet RA, Wang Y, et al. Immunoprevention of KRAS-driven lung adenocarcinoma by a multipeptide vaccine. Oncotarget 2017;8(47):82689–99 doi 10.18632/oncotarget.19831.. [PubMed: 29137294]
43. Stankevicius V, Vasauskas G, Bulotiene D, Butkyte S, Jarmalaite S, Rotomskis R, et al. Gene and miRNA expression signature of Lewis lung carcinoma LLC1 cells in extracellular matrix enriched microenvironment. BMC Cancer 2016;16(1):789 doi 10.1186/s12885-016-2825-9. [PubMed: 27729023]
44. Viitala M, Virtakoivu R, Tadayon S, Rannikko J, Jalkanen S, Hollmen M. Immunotherapeutic Blockade of Macrophage Clever-1 Reactivates the CD8(+) T-cell Response against Immunosuppressive Tumors. Clin Cancer Res 2019;25(11):3289–303 doi 10.1158/1078-0432.CCR-18-3016. [PubMed: 30755440]
45. Stewart DJ. Wnt signaling pathway in non-small cell lung cancer. J Natl Cancer Inst 2014;106(1):djt356 doi 10.1093/jnci/djt356. [PubMed: 24309006]
46. Lloyd CM, Marsland BJ. Lung Homeostasis: Influence of Age, Microbes, and the Immune System. Immunity 2017;46(4):549–61 doi 10.1016/j.immuni.2017.04.005. [PubMed: 28423336]
47. Jain P, Jain C, Velcheti V. Role of immune-checkpoint inhibitors in lung cancer. Ther Adv Respir Dis 2018;12:1753465817750075 doi 10.1177/1753465817750075. [PubMed: 29385894]
48. Vollmer J, Weeratna R, Payette P, Jurk M, Schetter C, Laucht M, et al. Characterization of three CpG oligodeoxynucleotide classes with distinct immunostimulatory activities. Eur J Immunol 2004;34(1):251–62 doi 10.1002/eji.200324032. [PubMed: 14971051]
49. Kashyap AS, Thelemann T, Klar R, Kallert SM, Festag J, Buchi M, et al. Antisense oligonucleotide targeting CD39 improves anti-tumor T cell immunity. J Immunother Cancer 2019;7(1):67 doi 10.1186/s40425-019-0545-9. [PubMed: 30871609]
50. Blanco MA, Aleckovic M, Hua Y, Li T, Wei Y, Xu Z, et al. Identification of staphylococcal nuclease domain-containing 1 (SND1) as a Metadherin-interacting protein with metastasis-promoting functions. J Biol Chem 2011;286(22):19982–92 doi 10.1074/jbc.M111.240077. [PubMed: 21478147]
51. Gnosa S, Shen YM, Wang CJ, Zhang H, Stratmann J, Arbman G, et al. Expression of AEG-1 mRNA and protein in colorectal cancer patients and colon cancer cell lines. J Transl Med 2012;10:109 doi 10.1186/1479-5876-10-109. [PubMed: 22643064]
52. Gnosa S, Ticha I, Haapaniemi S, Sun XF. MTDH genetic variants in colorectal cancer patients. Sci Rep 2016;6:23163 doi 10.1038/srep23163. [PubMed: 26983693]

53. Song HT, Qin Y, Yao GD, Tian ZN, Fu SB, Geng JS. Astrocyte elevated gene-1 mediates glycolysis and tumorigenesis in colorectal carcinoma cells via AMPK signaling. Mediators Inflamm 2014;2014:287381 doi 10.1155/2014/287381. [PubMed: 24829520]

54. Zhang F, Yang Q, Meng F, Shi H, Li H, Liang Y, et al. Astrocyte elevated gene-1 interacts with beta-catenin and increases migration and invasion of colorectal carcinoma. Mol Carcinog 2013;52(8):603–10 doi 10.1002/mc.21894. [PubMed: 22431469]

55. Yoo BK, Emdad L, Su ZZ, Villanueva A, Chiang DY, Mukhopadhyay ND, et al. Astrocyte elevated gene-1 regulates hepatocellular carcinoma development and progression. J Clin Invest 2009;119(3):465–77 doi 10.1172/JCI36460. [PubMed: 19221438]

56. Jian-bo X, Hui W, Yu-long H, Chang-hua Z, Long-juan Z, Shi-rong C, et al. Astrocyte-elevated gene-1 overexpression is associated with poor prognosis in gastric cancer. Med Oncol 2011;28(2):455–62 doi 10.1007/s12032-010-9475-6. [PubMed: 20300973]

57. Frieden M, Orum H. Locked nucleic acid holds promise in the treatment of cancer. Curr Pharm Des 2008;14(11):1138–42 doi 10.2174/138161208784246234. [PubMed: 18473860]

Significance:

This study provides new insights into the mechanism of MTDH in promoting colorectal and lung cancers, as well as genetic and pharmacological evidence supporting the development of MTDH-targeting therapeutics.

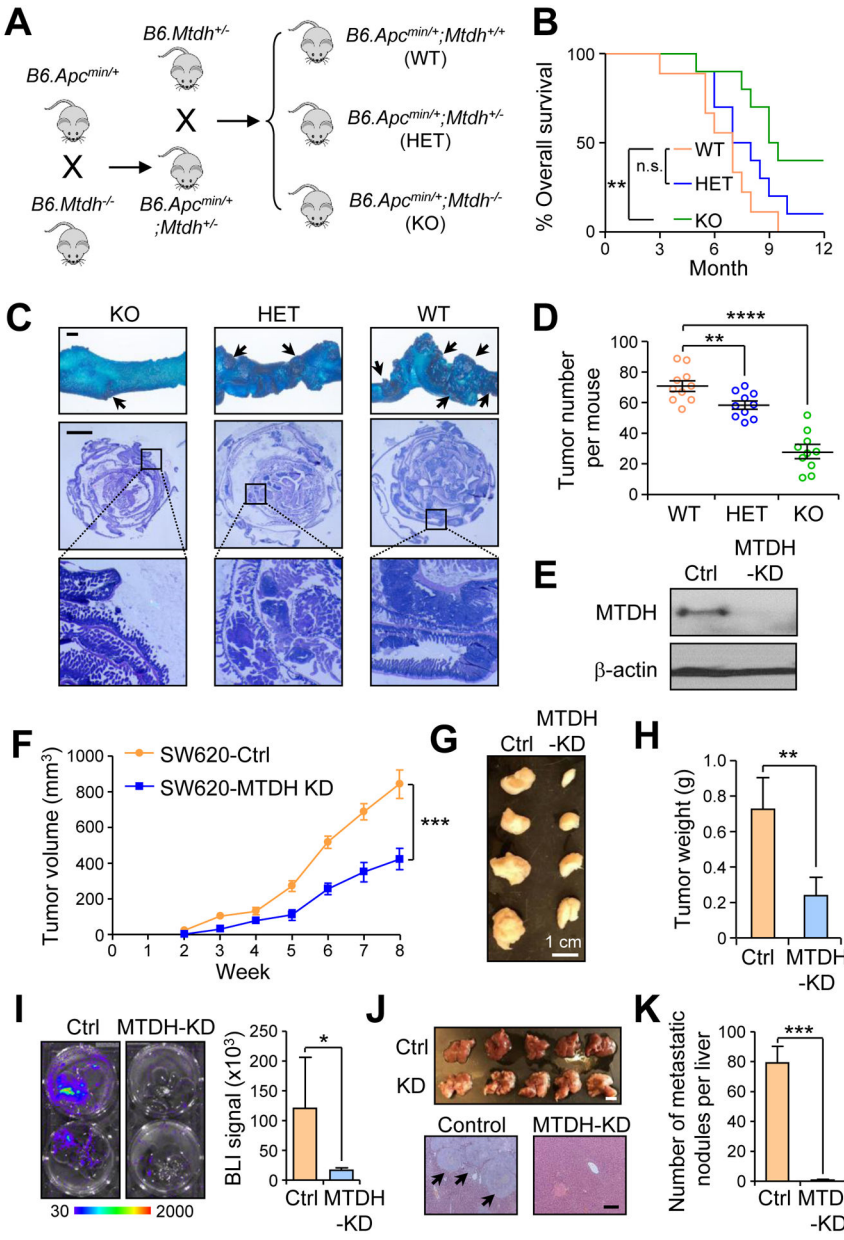

Figure 1.

MTDH promotes colorectal cancer progression and metastasis. **A,** Schematic diagram of the generation of *B6.APC*$^{min/+}$ mice with *Mtdh*$^{+/+}$ (WT), *Mtdh*$^{+/-}$ (HET), or *Mtdh*$^{-/-}$ (KO) background. **B,** Kaplan-Meier overall survival curve of the indicated mouse strains was plotted. n=10 mice per group. p value by log-rank tests. **C,** Representative images of the intestines collected from indicated groups at the age of 6 months. The intestines were subjected to methylene blue (top) or H&E staining (middle and bottom). Arrows indicate tumor nodules. Size bars, 5 mm. **D,** Tumor nodules in intestines from (**C**) were counted. n=10 mice per group. **E,** Knockdown (KD) efficiency of MTDH in SW620 cells was evaluated with western blot. **F,** 100k of control and MTDH-KD SW620 cells stably expressing firefly luciferase were injected into male NSG mice subcutaneously. Primary

tumors were measured once per week. n=6 mice per group. **G** and **H,** Representative primary tumors collected from (**F**) at endpoint are shown (**G**) and were weighed (**H**). **I,** Livers from mice in (**F**) were collected at the endpoint. Spontaneous liver metastasis was quantified by *ex vivo* bioluminescent imaging (BLI). n=6 livers per group. **J** and **K,** 100k of control or MTDH-KD SW620 cells were injected into the spleen of NSG mice. 5 weeks after injection, mice were euthanized and livers were collected to evaluate liver metastasis. Representative livers and H&E staining are shown (**J**). Liver metastatic nodules were counted (**K**). Size bars: 1 cm (livers) and 100 μm (H&E). n=5 mice per group. Data represent mean ± SEM. n.s. $p>0.05$, *$p<0.05$, **$p<0.01$, ***$p<0.001$, ****$p<0.0001$. Significance determined by one-way ANOVA test (**D**), longitudinal models (**F**), or two tailed Student's *t*-test (**H**, **I**, **K**).

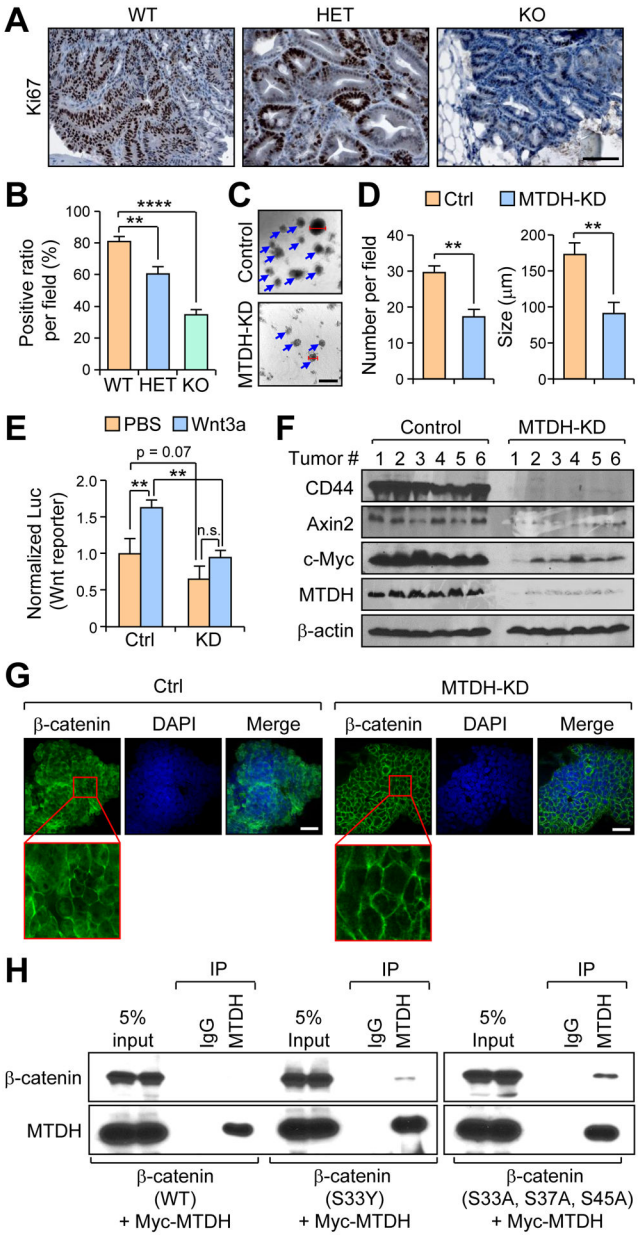

Figure 2.

MTDH facilitates nuclear localization of β-catenin and activates Wnt signaling. **A** and **B,** Intestines collected from *B6.APC*$^{min/+}$;*Mtdh*$^{+/+}$ (WT), *B6.APC*$^{min/+}$;*Mtdh*$^{+/-}$ (HET), and *B6.APC*$^{min/+}$;*Mtdh*$^{-/-}$ (KO) were subjected to Ki67 immunohistochemistry (IHC) staining. Representative images are shown (**A**). Ki67 positive ratios were quantified (**B**). n=9 intestines per group. Size bar: 50 μm. **C,** 2k of control (Ctrl) or MTDH-KD SW620 cells were employed for 3D culture in 6-well low attachment plates. Three fields of each well were randomly picked. Representative images of the field in each group are shown. Size bar: 100 μm. **D,** The numbers of solid and round spheres as indicated with blue arrows in (C) were counted. The diameters of these counted spheres, as indicated by red lines in (C), were measured to quantify sphere size. The average of three independent experiments are shown.

E, Control or MTDH-KD SW620 cells were treated with PBS or 500 ng/ml of recombinant Wnt3a protein for 6 hr. The activity of Wnt signaling was evaluated by the Wnt reporter assay. **F,** Primary tumors formed by control or MTDH-KD SW620 cells were collected and Wnt activation was evaluated by western blot with antibodies detecting the indicated Wnt pathway targets. **G,** Control or MTDH-KD SW620 cells were used for 3D culture. 10 days after culture, the spheres were collected for immunofluorescent staining with a β-catenin-specific antibody and DAPI. Size bar: 50 μm. **H,** Myc-MTDH and indicated β-catenin plasmids were co-transfected into HEK293T cells. 48 hr after transfection, cells were collected and lysates were prepared followed by immunoprecipitation assay. The samples were analyzed by western blot. Data represent mean ± SEM. n.s. $p>0.05$, **$p<0.01$, ****$p<0.0001$. Significance determined by one-way ANOVA test (**B**, **E**) and two tailed Student's *t*-test (**D**).

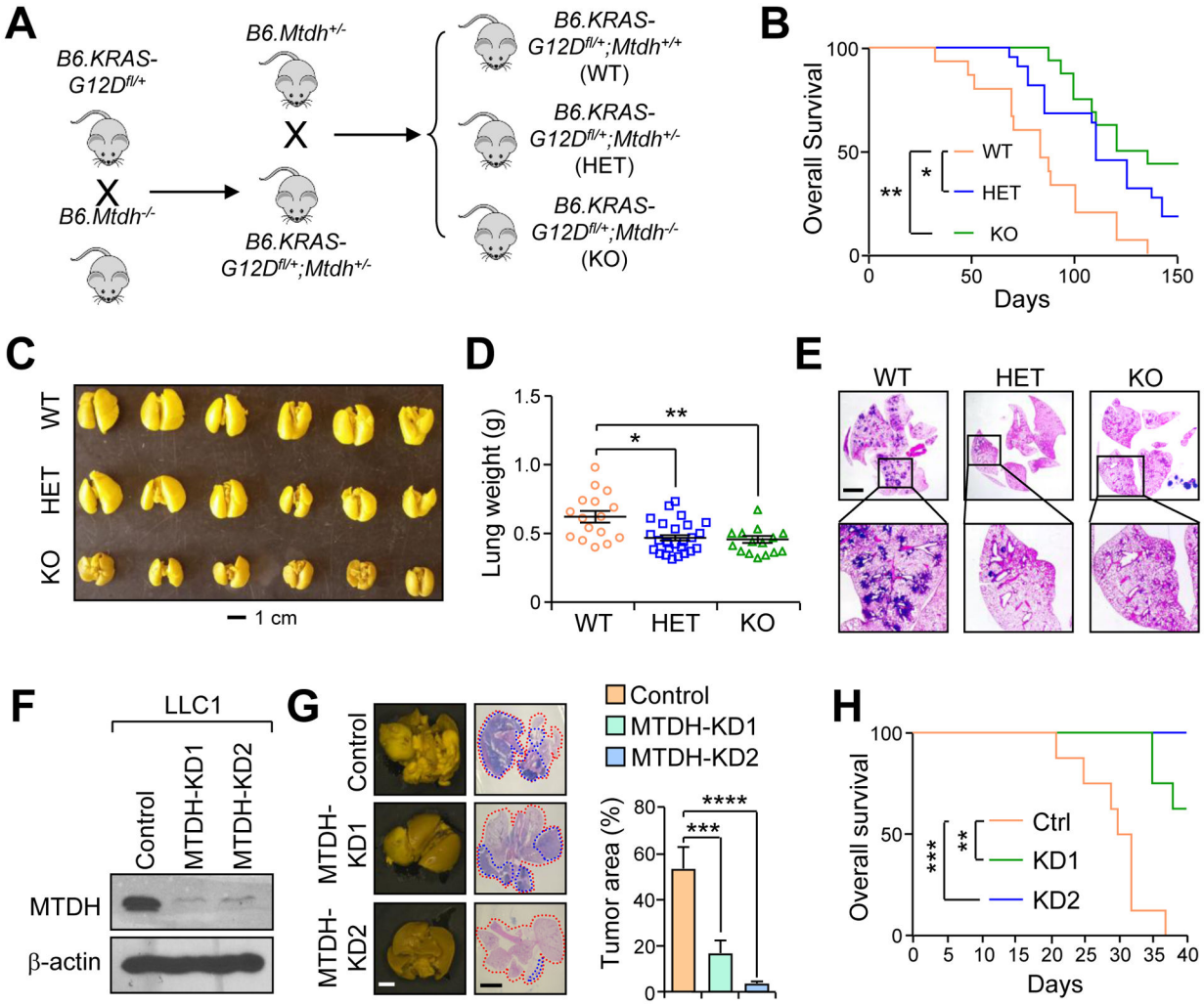

Figure 3.

MTDH promotes lung cancer progression. **A,** Schematic diagram of generation of *B6.KRAS-G12D*$^{fl/+}$ mice with *Mtdh*$^{+/+}$ (WT), *Mtdh*$^{+/-}$ (HET), or *Mtdh*$^{-/-}$ (KO). **B,** Indicated 6-week old mice were treated with Adeno-Cre virus by intranasal infection. The overall survival of the mice was plotted after the treatment. WT=16 mice; HET=22 mice; KO=16 mice. **C** and **D,** Representative lungs are shown (**C**) and weights were measured (**D**). WT=16 mice; HET=25 mice; KO=15 mice. **E,** Lungs were collected and H&E staining was performed. Size bar: 5 mm. **F,** Western blot analysis of endogenous MTDH KD in LLC1 cells. **G,** 200k of control and MTDH-KD LLC1 cells were injected into 8 weeks male C57BL/6 (B6) mice. Lungs were collected, H&E staining was performed. Total lung and tumor areas were highlighted with red and blue dash circles respectively. The areas were quantified with ImageJ and the tumor ratio (%) was determined as (tumor area)/(total lung area)x100%. n=8 mice per group. Size bars: 5 mm. **H,** The overall survival of the mice after tumor injection in (**G**) was plotted. n=8 mice per group. Data represent mean ± SEM. *p<0.05, **p<0.01, ***p<0.001, ****p<0.0001. Significance determined by one-way ANOVA test (**D**, **G**) and log-rank tests (**B**, **H**).

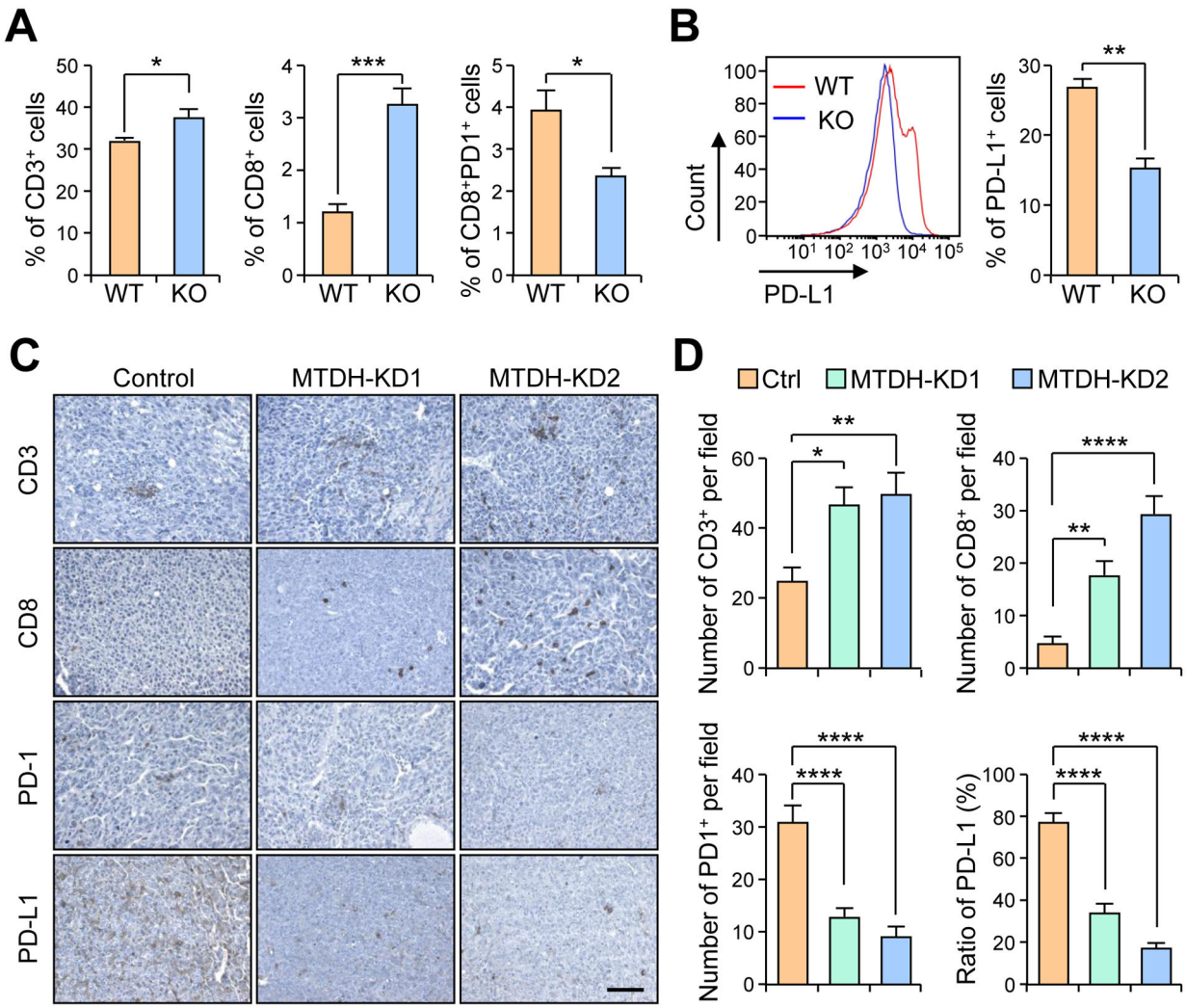

Figure 4.

MTDH enhances PD-L1 expression and decreases T cell infiltration in lung tumors. **A** and **B,** Lungs with tumors from *B6.KRAS-G12D*$^{fl/+}$;*Mtdh*$^{+/+}$ (WT) and *B6.KRAS-G12D*$^{fl/+}$;*Mtdh*$^{-/-}$ (KO) mice were collected for flow cytometry analysis. Positive ratios of CD3$^+$ in CD45 population, CD8$^+$ in CD3 population, and PD1$^+$ in CD8 population were quantified (**A**). The expression of PD-L1 in live cell populations was also examined (**B**). WT=3 lungs; KO=5 lungs. **C** and **D,** LLC1 lung tumors formed by control (Ctrl) or MTDH-KD cells were collected and were subjected to IHC staining with indicated antibodies (**C**). Number of positive cells or positive ratio per field were quantified (**D**). n=8 lungs per group. Size bar: 50 μm. Data represent mean ± SEM. *p<0.05, **p<0.01, ***p<0.001, ***p<0.0001. Significance determined by two tailed Student's *t*-test (**A**, **B**) and one-way ANOVA test (**D**).

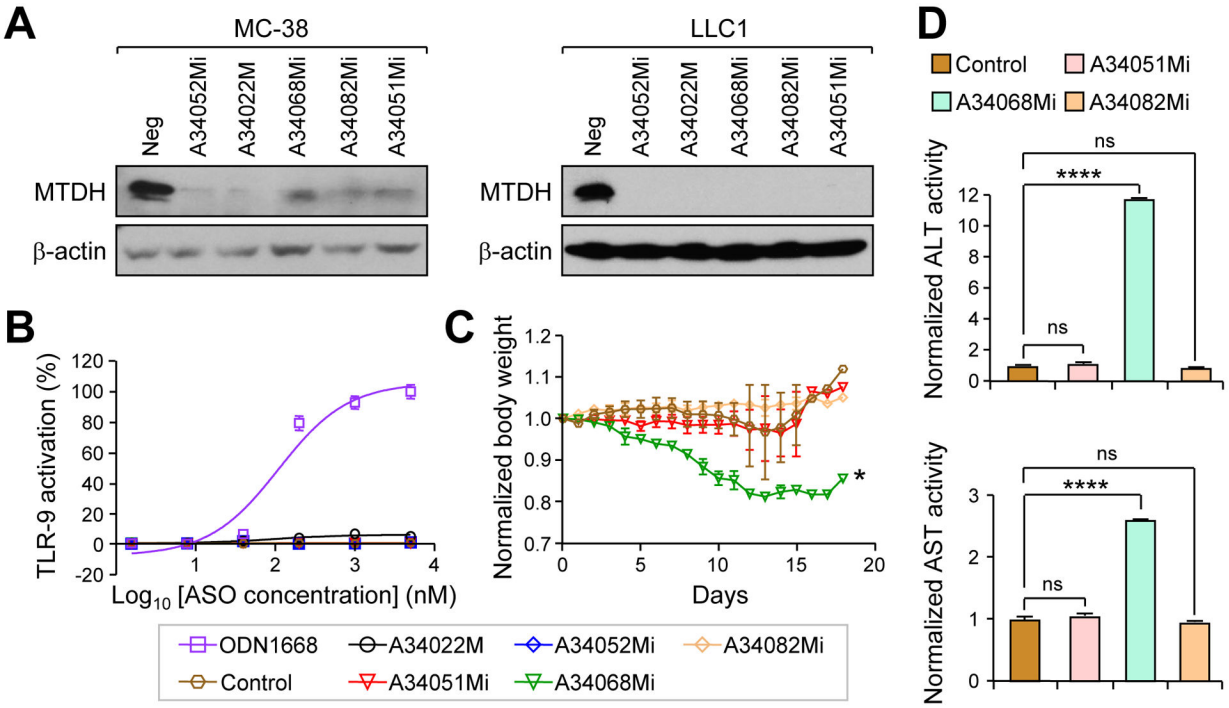

Figure 5.

Screening MTDH antisense oligonucleotides (ASOs) for *in vivo* treatment. **A,** MC-38 and LLC1 cells were treated with 5 μM of the five selected ASOs or the control oligonucleotide for three days. The cells were then collected and MTDH protein expression was evaluated with western blot. **B,** TLR9 activation assay was performed to assess the pro-inflammatory potential of the five ASOs in a TRL9 NF-κB reporter system. ODN1668 was used as a positive control. **C,** Balb/C mice were treated with 20 mg/kg of the indicated ASOs via intraperitoneal (i.p.) injection for 18 days (treatment scheme shown in Supplementary Fig. S4D). The body weight was measured daily. * indicates significant body weight loss. **D,** At endpoint, serum from treated mice was collected. AST (Sigma-Aldrich, MAK055) and ALT (Sigma-Aldrich, MAK052) was measured to determine liver toxicity. Data represent mean ± SEM. *p<0.05, ****p<0.0001. Significance determined by two tailed Student's *t*-test (**C**) and one-way ANOVA test (**D**).

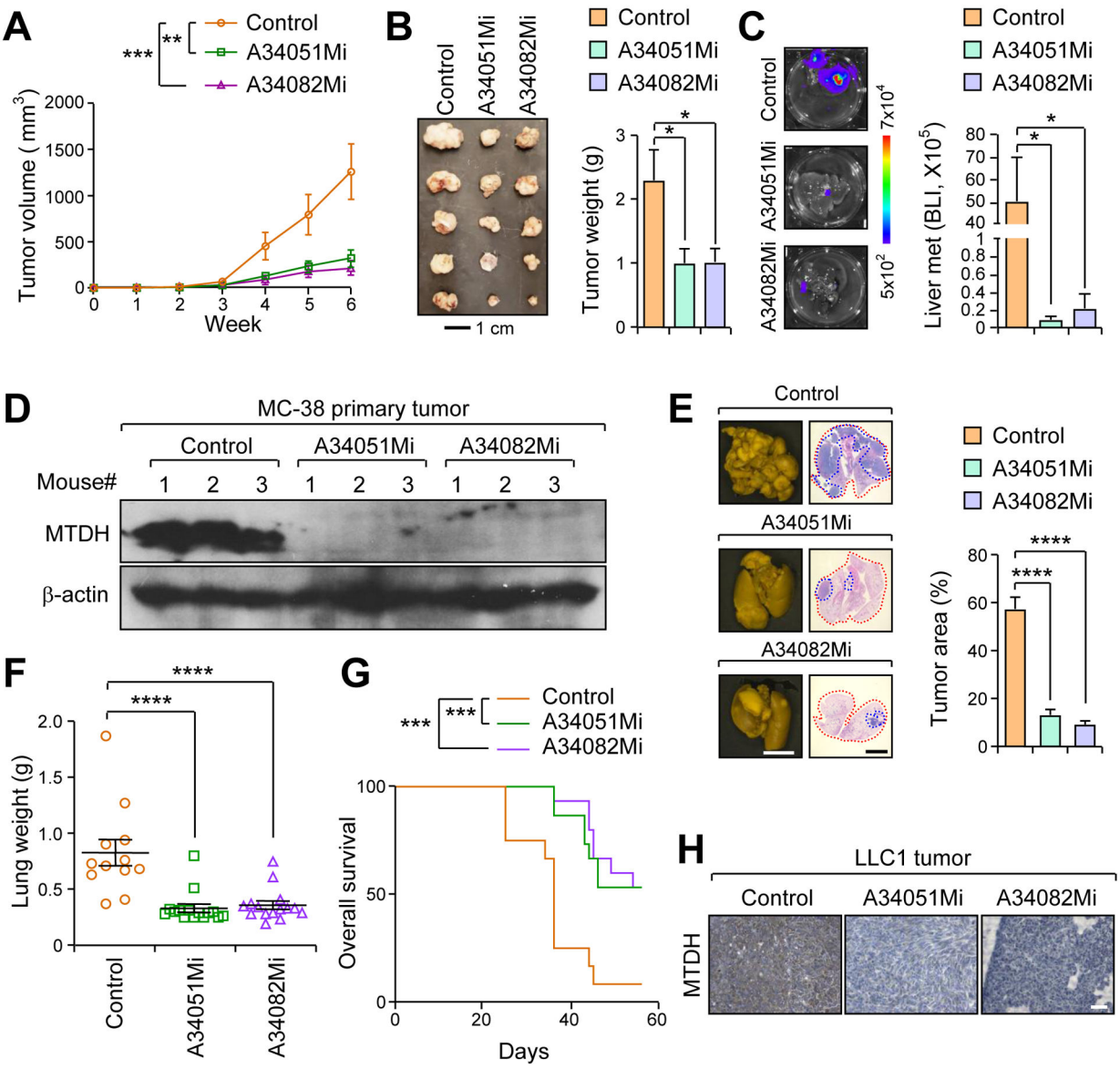

Figure 6.

MTDH-ASO treatments significantly suppress cancer progression and metastasis. **A,** 250k of MC-38 cells stably expressing firefly luciferase were injected into C57BL/6 mice subcutaneously. After the primary tumors had been well established, the mice were randomized and treated with 20 mg/kg of indicated MTDH ASOs or negative control via i.p. injection. After a treatment period of 6 weeks, the primary tumor volumes were measured weekly. n=12 mice per group. **B,** Representative tumors are shown (left panel) and weights were measured (right panel). n=10 tumors per group. **C,** Livers were collected and spontaneous metastasis was quantified by *ex vivo* BLI. Control=12 livers, A34051Mi=10 livers, A34082Mi=12 livers. **D,** Primary tumors were collected and MTDH expression was evaluated by western blot. **E,** C57BL/6 mice were injected with 100k of LLC1 cells intravenously. One week after injection, the mice were randomized and treated with negative control, A34051Mi, or A34082Mi. Lungs were collected and H&E staining was performed

to determine the tumor area. Total lung and tumor areas were highlighted with red and blue dash circles respectively. The areas were quantified with ImageJ and the tumor ratio (%) was determined as (tumor area)/(total lung area)x100%. Control =12 lungs, A34051Mi =15 lungs, A34082Mi =15 lungs. Size bar: 5 mm. **F,** Lungs from each group were weighed. Control =12 lungs, A34051Mi =15 lungs, A34082Mi =15 lungs. **G,** Kaplan-Meier overall survival curve after treatments was plotted. Control =12 mice, A34051Mi =15 mice, A34082Mi =15 mice. **H,** The lungs were then collected for IHC staining to determine MTDH expression at endpoint. Data represent mean ± SEM. *p<0.05, **p<0.01, ***p<0.001, ****p<0.0001. Significance determined by one-way ANOVA test (**A-C**, **E**, **F**) or log-rank tests (**G**).

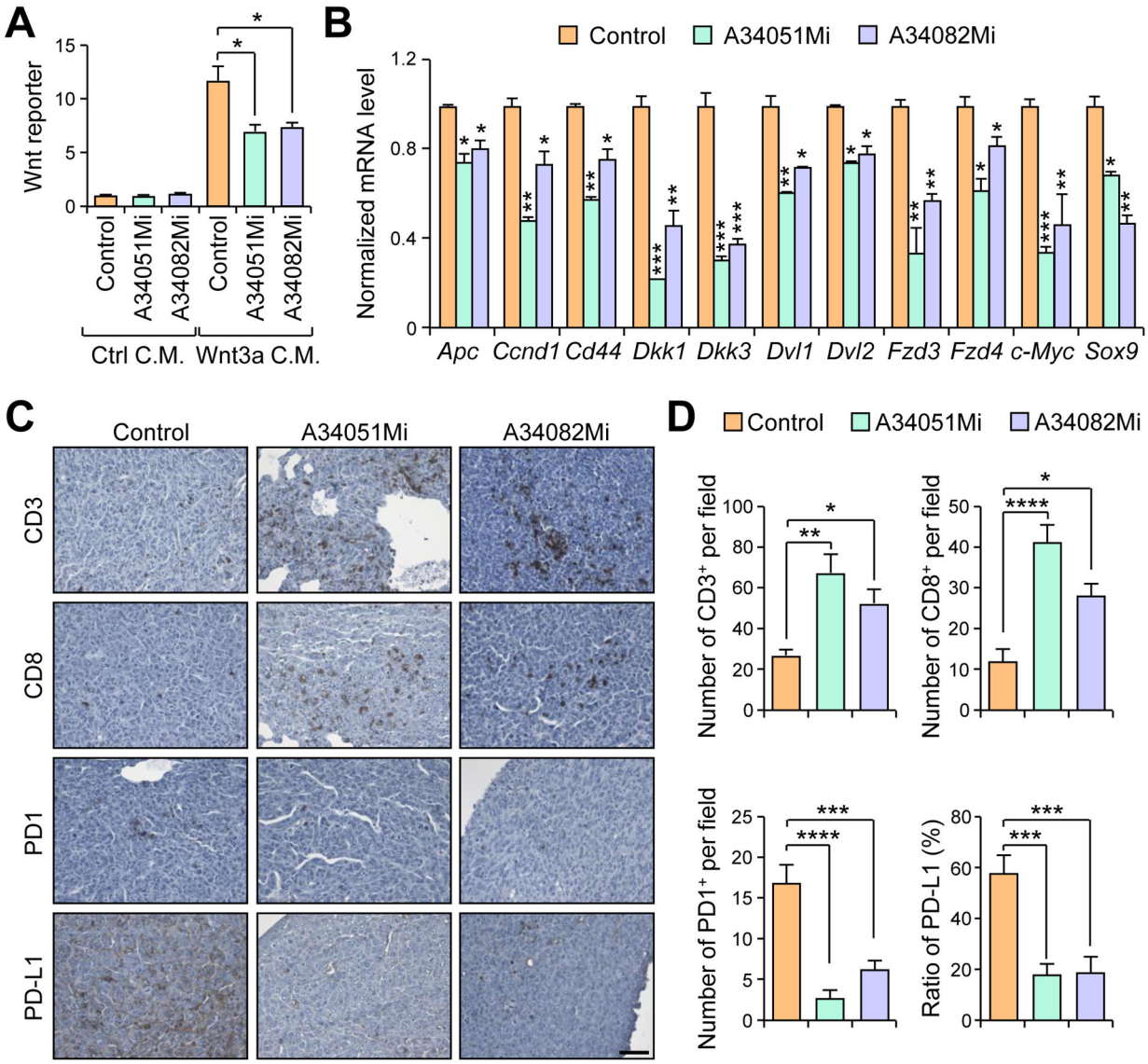

Figure 7.

MTDH-ASO treatments suppress Wnt activation in colorectal cancer and enhance T cell infiltration in lung cancer. **A,** MC-38 cells pre-treated with 5 μM of negative control, A34051Mi, or A34082Mi for three days were treated with control-conditioned media (Ctrl C.M.) or Wnt3a-conditioned media (Wnt3a C.M.) for another 6 hr. The Wnt activation was then determined by the Wnt reporter assay. **B,** MC-38 primary tumors from mice that had been treated with negative control, A34051Mi, or A34082Mi were collected. Total RNA was extracted followed by qRT-PCR to determine the expression of Wnt downstream genes. n=3 tumors per group. **C** and **D,** LLC1 tumors from mice that had been treated with negative control, A34051Mi, or A34082Mi were subjected to IHC staining with the indicated antibodies (**C**). The number or percentage of positive cells was quantified (**D**). n=6 lungs per group. Size bar: 50 μm. Data represent mean ± SEM. *p<0.05, **p<0.01, ***p<0.001, ****p<0.0001. Significance determined by one-way ANOVA test.